

EFFICIENCY ENHANCEMENT IN A TAPERED FREE ELECTRON LASER BY VARYING THE ELECTRON BEAM RADIUS*

Y. Jiao[#], J. Wu, SLAC, Menlo Park, CA 94025, USA

Q. Qin, IHEP, Beijing 100049, P.R. China

Abstract

Energy extraction efficiency of a free electron laser (FEL) can be greatly increased using a tapered undulator and self-seeding. An in-depth understanding of the tapering-related physics is required to explore the full potential of a tapered FEL, not only by tapering the undulator parameters in longitudinal dimension, but also optimizing the transverse effects. Based on the modified one-dimensional FEL model and GNESIS single-frequency numerical simulations, we study the contribution of variation in electron beam radius and related transverse effects. Taking a terawatt-level, 120-m, hard X-ray, tapered FEL as example, we demonstrate that a reasonably varied, instead of a constant, electron beam radius along the undulator helps to improve the optical guiding and hence the radiation output.

INTRODUCTION

Recent results on single pulse coherent diffraction imaging of proteins [1] and viruses [2] using an X-ray free electron laser (FEL) show that the resolution can be improved by both increasing the number of the coherent photons and simultaneously reducing the pulse duration to about 10 femtoseconds (fs) or less, thus requiring a peak power of one terawatt (TW) or larger compared to the present values of 20 to 50 GW available at saturation from the self-amplified spontaneous emission (SASE) mode. Theoretical work done at DESY [3] and SLAC [4] shows that one way to increase the peak radiation power of a SASE X-ray FEL to the TW level is to use a tapered undulator, following a concept initially proposed by Kroll, Morton and Rosenbluth (KMR) [5], together with the self-seeding option [6].

The SLAC work shows the existence of a saturation effect that limits the efficiency of energy transfer from the electrons to the radiation to values below those predicted by the one-dimensional (1D) KMR theory [7, 8]. The work is based on numerical simulations, using the three-dimensional (3D), time dependent codes GENESIS [9] and GINGER [10]. Studies suggest that the saturation effect is due to some combination of diffraction, refraction, radial dependence of the radiation field, and time dependent, slippage effects.

Better understanding of the limits and capabilities of a self-seeded tapered FEL requires an in-depth study of the 3D effects, in particular diffraction and refraction, absent from the 1D KMR analysis. While GENESIS and GINGER have been benchmarked against many

experimental results and give a reliable evaluation of FEL performance, they require moderately long computing time, limiting the possibility of multi-dimensional, parametric optimization of FEL performance when 3D and time dependent effects are important. To this end we have developed a model of a tapered FEL, using the 1D KMR theory and the optical fiber approximation to describe 3D effects and optical guiding [11-14]. While the model contains some approximations, it allows us to explore the full potential of a high-peak-power FEL not only by tapering the undulator parameters in longitudinal dimension but also by optimizing the transverse effects.

PHYSICAL MODEL

Formulation

We have developed a modified 1D FEL physical model in Ref. [15]. A relatively simple introduction of the model is presented here. KMR use the Hamiltonian approach to derive the equations that describe the electrons' synchrotron oscillations in the bucket associated with the ponderomotive potential in terms of the wiggler magnetic field, wiggler period and radiation field [5]. The introduction of the synchronous phase Ψ_r is used to formulate both the deceleration rate and the electron trapping fraction F_r . However, the theory is one-dimensional, and does not include any transverse effect.

By contrast, the optical guiding approach considers many important transverse effects. As shown in Refs. [11, 12], coherent interaction between the radiation and electrons can optically guide and focus the light. Because of its microbunching, the electron beam has an effective complex index of refraction n ,

$$n = 1 + \frac{\omega_{p0}^2 r_{b0}^2}{\omega_s^2 r_b^2} \frac{a_w}{2 |a_s|} [JJ] \left\langle \frac{e^{-i\Psi}}{\gamma} \right\rangle, \quad (1)$$

where ω_p is the electron plasma frequency, $\omega_s = k_s c$ is the radiation frequency with $\lambda_s = 2\pi/k_s$ the radiation wavelength and c the speed of light, r_b is the electron beam radius, $a_w = |e|B_w/k_w mc^2$ and $a_s = |e|A_s/mc^2$ are the normalized vector potentials of the helical undulator and on-axis radiation field (an additional $2^{1/2}$ factor in denominator for a linearly polarized undulator). Further symbols include e for the elementary charge, mc^2 the rest mass energy of electron, B_w the undulator field amplitude and $\lambda_w = 2\pi/k_w$ the undulator period, $[JJ] = 1$ for helical undulator and $[JJ] = J_0(\kappa) - J_1(\kappa)$ for linearly polarized undulator with $\kappa = a_w^2/2(1 + a_w^2)$, γ the electron's Lorentz factor, Ψ the electron phase relative to the ponderomotive potential. Quantities with subscript 0 indicate the initial electron and radiation beam parameters. The free space

*Work supported by the Department of Energy under Contract No. DE-AC02-76SF00515.

[#]jiaoyi@slac.stanford.edu, jiaoyi@ihep.ac.cn. Yi Jiao is now working in IHEP, Beijing, China.

surrounding the electron beam, by contrast, has a refraction index of 1.

We include the transverse effects revealed by the optical guiding approach in the framework of the 1D KMR theory and formulate a physical model explicitly with several principal assumptions (see Ref. [15] for more details).

Under the standard eikonal approximation, the normalized vector potential of the radiation field a_s is

$$a_s(r, z) = a_{s0}(z) e^{i\phi(r, z)} e^{\frac{-r^2}{r_s^2(z)}}, \quad (2)$$

where a_{s0} and ϕ are the slowly-varying on-axis amplitude and phase of the radiation field, respectively.

Similarly, we presume the initial electron beam profile obeys Gaussian distribution,

$$f_0(r) = \frac{N_e}{\pi r_{b0}^2} e^{-\frac{r^2}{r_{b0}^2}}, \quad (3)$$

where $N_e = \int_0^{r_{b0}} 2\pi r dr$ is the initial electron population.

Both a_{s0} and r_s will vary with z in a tapered FEL [12, 13]. From energy conservation, the changes in $a_{s0}(z)$ and $r_s(z)$ in a small longitudinal distance Δz follow

$$2a_{s0}^2(z_1)r_s(z_1)\Delta r_s(z) + 2r_s^2(z)a_{s0}(z)\Delta a_{s0}(z) \approx -\frac{\omega_{p0}^2}{\omega_s^2} r_{b0}^2 F_t(z) \gamma_r'(z) \Delta z, \quad (4)$$

where the prime refers to the z -derivative. In Eq. (5), the first and second terms on the LHS are proportional to the radiation power increment due to radial expansion and growth in on-axis field, respectively. In following discussion, we denote them as $\Delta E_r(\text{rad})$ and $\Delta E_a(\text{rad})$. Similarly we represent the term on the RHS as $\Delta E(e^-)$.

The evolution of r_s follows the envelope equation [12]

$$r_s'' + K^2 r_s = 0, \quad (5)$$

where the optical focusing parameter K^2 can be written in terms of the refractive guiding "fiber parameter" $V^2 = (n^2 - 1)k_s^2 r_b^2$ with on-axis $|a_s|$, the average of sine and cosine of Ψ , and $G(z) = (1-f)/(1+f)^2$ with the filling factor $f(z) = (r_b/r_s)^2$ [12],

$$K^2 = \frac{4}{k_s^2} (-1 + V^2 G + \frac{1}{4} V^4 G^2 \frac{\langle \sin \Psi \rangle}{\langle \cos \Psi \rangle^2} + \frac{1}{4} k_s r_s^2 \frac{d(V^2 G / \langle \cos \Psi \rangle)}{dz} \langle \sin \Psi \rangle) r_s^{-4}. \quad (6)$$

As mentioned, after the *initial saturation* in a tapered FEL, $\text{Re}(n) \approx 1$ and $\text{Im}(n) \ll 1$. Thus, in this region, V^2 can be written as [11, 13]

$$V^2(z) \approx \frac{\omega_{p0}^2 r_{b0}^2}{c^2} \frac{a_w}{a_{s0}} [JJ] \frac{\langle \cos \Psi \rangle}{\gamma_r}. \quad (7)$$

In Eqs. (6) and (7), $\langle \sin \Psi \rangle$ and $\langle \cos \Psi \rangle$ are approximated by a radial average over only the trapped electrons [see Eq. (15)]. In Eq. (7), we assume that all the

trapped electrons lie exactly at the resonant energy $\gamma_r mc^2$, with γ_r in the form [5]

$$\gamma_r^2(z) = \frac{k_s}{2k_w(z)} (1 + a_w^2(z)). \quad (8)$$

To determine the radial distribution of the trapped electrons, we follow Ref. [5] to formulate the r -dependent synchronous phase Ψ_r in the form

$$\sin[\Psi_r(r, z)] = \frac{-\gamma_r(z) \gamma_r'(z)}{a_w(z) k_s |a_s(r, z)|}. \quad (9)$$

The local trapping fraction is given by

$$F_t(r, z) = \frac{\Psi_2(r, z) - \Psi_1(r, z)}{2\pi}, \quad (10)$$

where Ψ_1 and Ψ_2 are the minimum and maximum of the ponderomotive bucket,

$$\Psi_2(r, z) = \pi - \Psi_r(r, z), \quad \cos \Psi_1(r, z) + \Psi_1(r, z) \sin \Psi_r(r, z) = \quad (11)$$

$$\cos \Psi_2(r, z) + \Psi_2(r, z) \sin \Psi_r(r, z).$$

Note that $F_t(r, z) = 0$ when $\Psi_r(r, z) = \pi/2$.

Combining Eqs. (2), (10) and (11), one can see there is a maximum r beyond which there can be no trapped electrons, whose value is given by

$$r_{\max}(z) = r_s(z) \{-\ln[\sin \Psi_r(r=0, z)]\}^{1/2} = r_s(z) \{-\ln[\frac{-\gamma(z) \gamma'(z)}{a_w(z) k_s a_{s0}(z)}]\}^{1/2}. \quad (12)$$

Locally, the number of the trapped electrons is $F_t(r, z) f_0(r)$, the overall electron trapping fraction $F_t(z)$ is then obtained by averaging $F_t(r, z)$ over all r from 0 to r_{\max} ,

$$F_t(z) = \frac{1}{N_e} \int_0^{r_{\max}} F_t(r, z) f_0(r) 2\pi r dr, \quad (13)$$

Similarly, $\langle \cos \Psi \rangle$ (and similarly $\langle \sin \Psi \rangle$) for the trapped electrons is given by

$$\langle \cos \Psi \rangle(z) = \frac{1}{N_e} \int_0^{r_{\max}} \cos \Psi_r(r, z) F_t(r, z) f_0(r) 2\pi r dr, \quad (14)$$

We assume the undulator taper begins from the *initial saturation* location. Starting from the electron and radiation beam parameters at *initial saturation* [15], especially $(a_{s0, \text{sat}}, r_{s, \text{sat}}, \Psi_{r, \text{sat}}, F_{t, \text{sat}})$, one can iterate Eqs. (2) through (15) to evolve these parameters in z along the undulator for a specific taper profile, without requiring the 6D phase space details of the electron and radiation beam distribution from a numerical simulation code.

IMPROVING OPTICAL GUIDING WITH VARIED TRANSVERSE FOCUSING

The presented model enables us to analyze the contribution of varying electron beam radius to the radiation output. Let us consider a gradually decreased r_b in the latter part of a tapered undulator. Compared to the

case with the same taper profile but a constant r_b , the factor G and hence the optical focusing parameter K^2 will be slightly larger, leading to increased optical focusing and to smaller r_s as well as smaller $\Delta E_r(\text{rad})$. For a given taper profile, Eq. (4) predicts a larger a_{s0} , resulting in smaller $\Psi_r(r=0)$ and higher $F_r(r=0)$ [see Eqs. (10) and (11)]. On the other hand, a smaller r_s leads to a smaller r_{max} [see Eq. (12)], causing a higher $\Psi_r(r)$ and smaller $F_r(r)$ for electrons at large r . Thus, the detrapping of the electrons around axis will detrap less rapidly. The stronger on-axis optical guiding on one hand will tend to lead to a more rapidly growing a_{s0} ; on the other hand, a smaller r_s will increase diffractive effects. If one squeezes r_b to too small a value such that the diffraction effect dominates, the energy extracted from the electron beam will contribute to rapid radial expansion of the radiation rather than growth in a_{s0} . Thus one expects there is an optimal value for a decreased r_b . We note that, since G has been close to 1 in the latter part of the tapered undulator (generally $r_s \sim 2-3r_b$), the expected change in G and overall optical guiding due to r_b -variation is rather small. Thus we expect only a relatively small improvement from an r_b -variation compared with what is attainable from optimizing the taper profile in z at fixed r_b .

To test the contribution of a varied r_b , for a 120-m, hard X-ray, tapered FEL, we start to decrease r_b from the 30 m location by linearly increasing quadupole strengths. Figs. 1 and 2 show the resulting on-axis $|a_s|$, r_s and F_t in comparison with the constant r_b case, obtained by the GENESIS single-frequency simulation and the physical model, respectively. Both approaches predict higher on-axis $|a_s|$ and smaller r_s at the end of the undulator with a varied r_b .

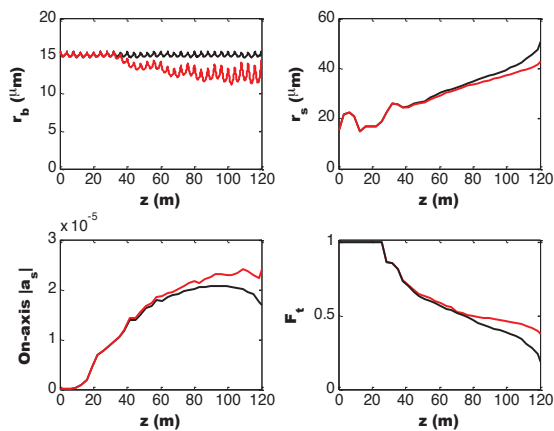


Figure 1: On-axis $|a_s|$, r_s and F_t with constant (black lines) and varied (red lines) r_b , obtained by GENESIS single-frequency simulation. The oscillation in r_b is due to imperfect matching of the transverse optics.

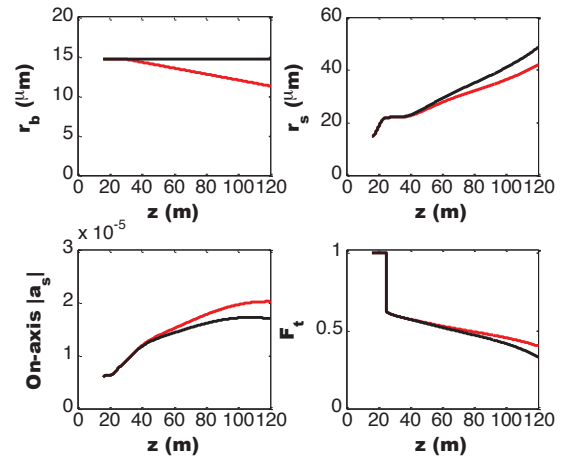


Figure 2: On-axis $|a_s|$, r_s and F_t with constant (black lines) and varied (red lines) r_b , obtained by the proposed physical model.

Simulations for the output radiation power are also performed. With a varied r_b , GENESIS single-frequency simulation predicts an increase in radiation power by a factor of 15%. When taking into account the time-dependent effects, sideband effect can limit the available maximum radiation power. Even though, squeezing r_b in this case helps to produce more radiation power at the end of the undulator (2.16 vs. 1.96 TW) or reach the same radiation power within a shorter undulator length (92 vs. 95 m for 1.5 TW), compared to the case of a constant r_b .

REFERENCES

- [1] H.N. Chapman et al., Nature 470 (2011) 73.
- [2] N.M. Seibert et al., Nature 470 (2011) 78.
- [3] G. Geloni, V. Kocharyan, and E. Saldin, DESY 10-108, 2010.
- [4] W.M. Fawley et al., FEL2011, TUOA4.
- [5] N.M. Kroll, P.L. Morton and M.N. Rosenbluth, IEEE J. Quantum Electron. 17 (1981) 1436.
- [6] G. Geloni, V. Kocharyan, and E. Saldin, DESY 11-049, 2011.
- [7] L.-H. Yu, Phys. Rev. A 44 (1991) 5178.
- [8] K.-J. Kim, LBL-31969, 1992.
- [9] S. Reiche, NIM. A 429 (1999) 243.
- [10] W.M. Fawley, LBID-2141, CBP Tech Note-104, UC-414, 1995.
- [11] E.T. Scharlemann, A.M. Sessler and J.S. Wurtele, Phys. Rev. Lett. 54 (1985) 1925.
- [12] P. Sprangle, A. Ting, and C.M. Tang, Phys. Rev. Lett. 59 (1987) 202.
- [13] B. Hafizi, A. Ting, P. Sprangle, and C.M. Tang, Phys. Rev. Lett. 64 (1990) 180.
- [14] W.M. Fawley, NIM. A 375 (1996) 550.
- [15] Y. Jiao et al., Phys. Rev. ST Accel. Beams 15 (2012) 050704.